JGR Space Physics

RESEARCH ARTICLE
10.1029/2020JA027906

Daily and Monthly Variations of the Equatorial Ionization Anomaly (EIA) Over the Brazilian Sector During the Descending Phase of the Solar Cycle 24

M. A. L. Dias[1,2], P. R. Fagundes[1], K. Venkatesh[3], V. G. Pillat[1], B. A. G. Ribeiro[1], G. K. Seemala[4], and M. O. Arcanjo[1]

[1]Laboratorio de Fisica e Astronomia, Universidade do Vale do Paraiba–UNIVAP, São José dos Campos, Brazil, [2]Observatorio de Fisica Espacial, Campus Araguatins, Instituto Federal de Tocantins–IFTO, Palmas, Brazil, [3]National Atmospheric Research Laboratory (NARL), Tirupati, India, [4]Indian Institute of Geomagnetism, Navi Mumbai, India

Key Points:
- Day-to-day and month-to-month characteristics of the EIA in three different longitudinal sectors over Brazil are studied for the first time
- Observations from three latitudinal networks with 35 GPS-VTEC stations spanning from the equator to low latitudes are analyzed
- The EIA features from GPS-VTEC measurements are compared with those from IRI-2016 model

Correspondence to:
P. R. Fagundes,
fagundes@univap.br

Citation:
Dias, M. A. L., Fagundes, P. R., Venkatesh, K., Pillat, V. G., Ribeiro, B. A. G., Seemala, G. K., & Arcanjo, M. O. (2020). Daily and monthly variations of the equatorial ionization anomaly (EIA) over the Brazilian sector during the descending phase of the Solar Cycle 24. *Journal of Geophysical Research: Space Physics*, *125*, e2020JA027906. https://doi.org/10.1029/2020JA027906

Received 12 FEB 2020
Accepted 15 JUL 2020
Accepted article online 6 AUG 2020

Abstract It has been noticed recently that the equatorial ionization anomaly (EIA) in the Brazilian eastern, middle, and western sectors present significant longitudinal variability within a short separation due to the presence of typical magnetic field structure over South America. Therefore, the main motivation of this study is to investigate day-to-day and month-to-month characteristics of the EIA in three closely spaced longitudinal sectors over the Brazilian region during the year 2016 in the descending phase of the solar activity. These three longitudinal sectors are perpendicular to the magnetic equator at its largest declination over the globe. The EIA showed a semiannual variation in all sectors with a major maximum during the summer, a minimum during the winter, and secondary maximum during spring. In addition, the EIA shows its classical behavior with a trough around the magnetic equator and crests at low latitudes (from ±15° to ±20°). When the EIA is not developed, the maximum ionization is located around the dip equatorial latitudes and the anomaly crest is absent. The number of days within 1 year that showed clear EIA development in the west, middle, and east sectors is 248 (78.2%), 236 (74.4%), and 265 (83.6%), respectively. The undeveloped/absence of EIA is also found often during the months of winter, and the numbers of such days during 2016 in the west, middle, and east are 69 (21.8%), 81 (25.6%), and 52 (16.4%), respectively. Also, the shape, strength, extent, and lifetimes of EIA crest have shown significant variabilities between the three sectors during different seasons. Further, a comparative analysis is carried out on the variations of EIA crest and lifetime between GPS observations and IRI-2016 model, and the results are discussed.

1. Introduction

It is well known that the equatorial ionosphere is characterized by the dynamic phenomena called the equatorial ionization anomaly (EIA). The day-to-day variability of EIA is controlled by several solar parameters, such as radiation (UV, EUV, and X-ray), solar activity, flares, and coronal mass ejection events. In addition, the neutral atmosphere (thermosphere) plays an important role in EIA day-to-day variations due to composition changes ($[O]/[N_2]$), thermospheric winds, and planetary, tide, and gravity waves (Romero-Hernandez et al., 2018). However, the equatorial F-region electrodynamics is the most important factor that controls the EIA day-to-day variability via fountain effect, as described below.

During the daytime, the equatorial and near-equatorial F-region present a vertical upward drift due to the special geometric configuration between the Earth's magnetic field ($\vec{B}$) and the zonal electric field component ($\vec{E}$). At the geomagnetic equator and the surrounding latitudes, the terrestrial magnetic field is parallel or almost parallel (north–south direction) to the Earth's surface, and its combination with the perpendicular daytime zonal electric field $\vec{E}_{eastward}$ yields the F-layer upward vertical drift that is given by Equation 1.

$$\vec{V}z_{upward} = \frac{\vec{E}_{eastward} \times \vec{B}_{northward}}{B^2} \quad (1)$$

The $\vec{V}z$ intensity depends on local time, longitude, and thermosphere-ionosphere coupling and exhibit significant variability from day-to-day, season, solar activity, and solar cycle. To explain different features in

the day-to-day variations of the $\vec{V}z$ drift, it is important to take into account the E- and F-region dynamos (Fejer et al., 1979). These two dynamos are also necessary to explain the enhancement of postsunset $\vec{E}_{eastward}$ just before it reverses to $\vec{E}_{westward}$, a phenomenon called as prereversal enhancement electric field (PRE).

Under the strong vertical drift over the equator, the F-region plasma reaches higher altitudes and diffuses downward along the magnetic field lines due to gravitational and pressure gradient forces. This is called as fountain effect, due to which a considerable portion of the plasma is removed from the magnetic equator and deposited at the low latitudes. This results in two EIA crests of plasma density—one in the northern magnetic hemisphere and the other in the southern magnetic hemisphere between ±15° and ±20° dip latitudes. It is important to mention that the plasma density crests are created due to the removal of the plasma density from the geomagnetic equator, which is deposited at the crests.

These EIA crests are not symmetric in both hemispheres due to the interaction between meridional thermosphere winds and F-region ionospheric plasma. When the meridional thermospheric neutral wind blows from pole to equator, the F-region moves upward. At higher altitudes, the neutral atmosphere has less density; therefore, neutral plasma recombination is less and the plasma density increases. On the other hand, in the hemisphere where the thermospheric wind blows from the equator to pole, the F-region plasma moves downward to lower altitudes where the neutral density increases and the recombination process is more effective, resulting in plasma density reduction.

The EIA shows signification variability in different spatial and temporal scales. Major factors that affect the EIA variability include the photochemical processes due to varying solar intensity, strength of the fountain effect, and the neutral wind magnitude and directions. The EIA seasonal variations and consequently the semiannual variation are controlled by subsolar point, thermosphere-ionosphere coupling, solar cycle, and F-region electrodynamics (fountain effect). As mentioned by Romero-Hernandez et al. (2018) several anomalies are important to be taken into account to understand the interhemispheric ionospheric seasonal behavior, such as winter, equinoctial, and annual anomalies. However, the ionosphere over the American region presents an extra complexity as compared with other sectors of the Earth due to a unique configuration of geographic and geomagnetic equators (Figure 1). Thus, all ionospheric phenomena that occur in this region of the Earth have a distinct and specific behavior, especially those that occur in the equatorial and low-latitude F-layer.

The ionospheric F-layer critical frequency (foF2) and peak height (hmF2) have been used to investigate the EIA variations over the Brazilian sector, and these parameters were then compared with International Reference Ionosphere (IRI) model data (Batista & Abdu, 2004; Bertoni et al., 2006). However, these studies used data from only two ionosondes, one located near-equatorial region and the other one near the EIA crest. Therefore, the details about the shape, lifetime, and strength of the EIA are limited by information from only two sites. Also, Jonah et al. (2015) investigated the total electron content (TEC) seasonal variation as a function of solar activity over the South American sector and noticed that during winter, the TEC values at the EIA crest are lower than at equatorial regions. They suggested that solar radiation during summer and equinox time is stronger than wintertime and that the fountain effect is not strong enough to transport the plasma from equator to low latitudes. Also, they mentioned that the meridional or zonal winds could be important to explain the changes in TEC.

Venkatesh, Fagundes, Seemala, et al. (2014) studied the EIA in the Brazilian eastern sector, using a chain of seven GPS-TEC receivers spanning from the equatorial region to low latitudes. They have shown that the EIA is developed during the southern summer and equinoxes with equatorial trough and low latitude crest while during wither, the EIA is absent with maximum ionization over the equator and absence of crest at low latitude. More recently, taking advantage of the increased number of GPS-TEC receivers over the Brazilian region, the EIA variations are studied in more detail using two chains of GPS-TEC receivers in the eastern and western Brazilian sectors, during some specific cases. In addition, Tardelli et al. (2018) studied the F-layer stratification into F3 and F4 at American southern crest of EIA.

The EIA was studied in other sectors and as well as in the Northern Hemisphere. Adebesin et al. (2018) investigated EIA trough in the African sector using ionosonde parameters (h′F, NmF2, and vertical plasma drift) using three equatorial sites and found NmF2 semiannual variation with the first peak in March and the

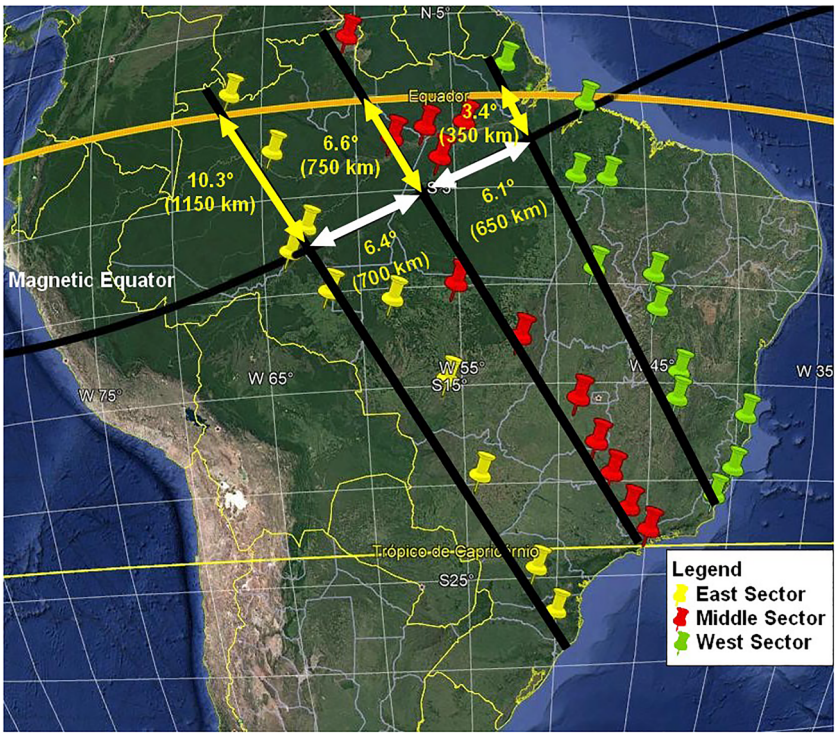

Figure 1. Map showing the 35 GPS-TEC stations used to study the EIA at eastern (green icons), middle (red icons), and western (yellow icons) Brazilian sectors. In addition, the distances between the geographic (yellow line) and geomagnetic (black line) equators and the distance among eastern, middle, and western Brazilian sectors are shown in km and degrees (lines with double arrows).

second peak in October/November. In addition, Seba et al. (2018) investigated the EIA climatology and its relationship with Spread-F over the African sector. Rao et al. (2018) studied the EIA variation using foF2 and compared with the IRI-2016 model in the Chinese sector. Khadka et al. (2018) studied the role of neutral wind and electric field on EIA asymmetry. In the Northern Hemisphere Indian sector, the crest shows maximum values during the equinox months and minimum values during the winter and summer (Kumar et al., 2014). Despite the proposal of Appleton (1946) that the EIA is characterized by a trough at magnetic equator and crests at about ±17 magnetic latitudes, it is important to investigate the spatial-temporal variation at different hemispheres and longitudes, especially over the American sector where the magnetic and geographic equators present a unique geometry.

In recent studies during geomagnetic storms and sudden stratospheric warming (SSW) events, it was reported that the EIA in the eastern and western Brazilian sectors presents different intensities, lifetimes, and morphologies (Fagundes et al., 2016; Ribeiro et al., 2019; Vieira et al., 2017). Even though the present study is not related with storms or SSW events, significant differences within a short longitudinal separation motivated us to study such variations during quiet-time conditions. Therefore, the present study carried out a detailed analysis of EIA variability in three sectors of the Brazilian territory during quiet conditions on the basis of day-to-day and month-to-month characteristics.

However, it is well known that the EIA plays an important role in the equatorial and low latitude regions, and its variability and strength are investigated to study how it affects other phenomena that occur in the equatorial region and low latitudes in the American, African, and Asian sectors. Those studies include aspects such as the EIA and fountain effect, EIA variations during the quiet and geomagnetic disturbed period, EIA and SSW, EIA and equatorial electrojet (EEJ), EIA and equatorial large-scale ionospheric irregularities, EIA and thermosphere winds, EIA and tides, EIA and traveling ionospheric disturbances (TIDs), and EIA and planetary waves.

In this investigation, we take advantage of the vertical TEC (VTEC) measurements from the Brazilian GPS network (http://www.ibge.gov.br/home/geociencias/geodesia/rbmc/rbmc_est.php) to explore the similarities

and differences in the EIA characteristics in three sectors (east, middle, and west) to investigate how the geometry of the equators affects the EIA crests and troughs. Besides, we compare the EIA characteristics from GPS-VTEC observations with those from IRI-2016 model outputs. The IRI-2016 model is widely used to predict several ionospheric parameters, including one of the most important ionospheric parameters, the TEC (Bilitza, 2001, 2018). As mentioned by Venkatesh, Fagundes, de Jesus, et al. (2014), comparative studies between the experimentally measured and IRI model-derived TEC have been carried out by several workers over different regions of the globe during different solar activity conditions (Abdu et al., 1996; Batista et al., 1994; Bhuyan & Borah, 2007; Bilitza et al., 1998; Oluwadare et al., 2019; Oyekola & Fagundes, 2012; Prasad et al., 2012).

Therefore, the main purpose of this study is to investigate for the first time the day-to-day and month-to-month characteristics of the EIA variations during a quiet time in three different longitudinal sectors over the Brazilian region, during the year 2016, descending phase of the Solar Cycle 24. It is interesting to mention here that the geomagnetic equator over Brazil presents the largest declination (Figure 1). As seen from Figure 1, the geographic and geomagnetic equators are quiet closer in the eastern sector, while they are largely separated in the western Brazilian sector. Further, the EIA month-to-month characteristics observed from GPS-VTEC measurements are compared with IRI-2016 modeled EIA features.

2. Data and Methodology

Figure 1 shows the South America map indicating the locations of the 35 GPS-TEC stations over Brazil used in the present work. The geographic and geomagnetic equators are shown by the yellow and black curves, respectively. Across the magnetic equator, there are three perpendicular black lines, and near these lines, the closest available GPS-TEC stations are indicated by pin marks. These selected GPS receivers along three different latitudinal chains over Brazil are used to investigate the similarities and differences of the EIA in these sectors. The green, red, and yellow pins indicate the GPS-TEC stations used in the east (from 39.7°W to 52.3°W), middle (from 45.1°W to 60.7°W) and west (from 50.3°W to 67°W) sectors, respectively. The station codes and geographic and geomagnetic latitudes of GPS receiver locations along the east, middle, and west sectors are listed in Table 1. The VTEC are analyzed from these three different latitudinal chains spanning from the equator to beyond the EIA crest along the eastern (13 stations), middle (12 stations), and western (10 stations) sectors over Brazil.

In addition, in Figure 1, the geometric configuration between the geographic and magnetic equators is highlighted in km and degrees by double-ended yellow arrows. The longitudinal distances between the black lines are shown by white arrows, which indicate that the considered three sectors are separated by approximately 700 km or about ~6°. In the east sector (green icons), the geographic and geomagnetic equators are nearer and the equatorial plasma fountain takes place close to the geographic equator, where the plasma production via photoionization is maximum during the daytime. On the other hand, in the west sector (yellow icons), the geographic and geomagnetic equators are separated by more than 1,100 km (~10°). This means that the equatorial plasma fountain occurs from the geographic low latitude, where the plasma production is lesser than that over the geographic equator.

The dual frequency measurements from GPS receivers are used to derive the TEC (measured in TECu $= 10^{16}$ el/m^2) values using the differential delay technique (Rama Rao et al., 2006; Seemala & Valladares, 2011; Venkatesh, Fagundes, de Jesus, et al., 2014). The difference in time delay between the frequencies L1 (1,575.42 MHz) and L2 (1,227.60 MHz) is given by

$$t_1 = 40.3\left(\frac{\mathrm{TEC}}{C f_1^2}\right) \text{ and } t_2 = 40.3\left(\frac{\mathrm{TEC}}{C f_2^2}\right) \tag{2}$$

$$\Delta t = \left(\frac{40.3}{C}\right)\frac{\mathrm{TEC}}{\left[\left(1/f_2^2\right) - \left(1/f_1^2\right)\right]} \tag{3}$$

where $\Delta t = t_2 - t_1$ and C is the speed of light. The slant TEC (STEC) thus derived is converted into VTEC using the relations

Table 1
The Station Names, Codes, Geographic Coordinates, and Dip Latitudes of the GPS-TEC Stations Over the Brazilian West, Middle, and East Sectors

GPS no.	Station name	Station codes	West sector geo. lat. (+N)	Geo. long. (+W)	Dip lat. (+N)
1	S. G. da Cachoeira	SAGA	−0.1	67.0	9.1
2	Tefe	AMTE	−3.3	64.7	5.5
3	Humaita	AMHA	−7.5	63.0	1.2
4	Porto Velho	POVE	−8.7	63.9	0.4
5	Ji-Parana	ROJI	−10.9	62.0	−2.2
6	Juina	MTJI	−11.4	58.7	−4.0
7	Cuiaba	CUIB	−15.5	56.1	−8.7
8	Campo Grande	MSCG	−20.4	54.5	−13.5
9	Guarapuava	PRGU	−25.4	51.5	−18.8
10	Lages	SCLA	−27.8	50.3	−21.1
GPS no.	**Station name**	**Station codes**	**Middle sector geo. lat. (+N)**	**Geo. long. (+W)**	**Dip lat. (+N)**
1	Boa Vista	BOAV	2.8	60.7	9.5
2	Itacoatira	ITAM	−3.1	58.4	3.2
3	Parintins	AMPR	−2.6	56.7	3.0
4	Santarem	PASM	−2.4	54.7	2.1
5	Itaituba	PAIT	−4.3	56.0	1.1
6	Colider	MTCO	−10.8	55.4	−4.9
7	Canarana	MTCN	−13.5	52.3	−8.9
8	Goiania	GOGY	−16.7	49.2	−13.2
9	Uberlandia	MGUB	−18.9	48.2	−15.6
10	Franca	SPFR	−20.5	47.4	−17.3
11	Inconfidentes	MGIN	−22.3	46.3	−19.3
12	Ubatuba	UBA1	−23.5	45.1	−20.8
GPS no.	**Station name**	**Station codes**	**East sector geo. lat. (+N)**	**Geo. long. (+W)**	**Dip lat. (+N)**
1	Laranjal do Jari	APLJ	−0.5	52.3	3.9
2	Macapa	MAPA	0.1	51.1	2.5
3	Belem	BELE	−1.4	48.4	−0.3
4	Maraba	MABA	−5.3	49.1	−3.5
5	Imperatriz	IMPZ	−5.5	47.5	−4.5
6	Palmas	TOPL	−10.2	48.3	−8.2
7	Corrente	PICR	−10.4	45.2	−10.2
8	Barreiras	BABR	−12.1	45.0	−11.8
9	Jaiba	JAMG	−15.3	43.8	−15.2
10	Montes Claros	MGMC	−16.7	43.8	−16.3
11	Teixeira de Freitas	BATF	−17.5	39.7	−19.4
12	Vitoria	CEFE	−20.3	40.3	−21.2
13	Campos Goytacazes	RJCG	−21.8	41.3	−21.7

$$\mathrm{VTEC} = [\mathrm{STEC} - (b_r - b_s)]/S(E) \tag{4}$$

$$S(E) = \frac{1}{\cos(Z)}\left[1 - \left(\frac{\cos(E)}{R_E + h_s}\right)^2\right]^{-1/2} \tag{5}$$

where b_r is the receiver bias, b_s is the satellite bias, STEC is the slant TEC, z is zenith angle of the satellite, R_E is the radius of the Earth, E is the elevation angle, and h_s is the ionospheric effective height above the Earth's surface.

First, the EIA day-to-day variability is investigated in the three different Brazilian sectors, and afterward, the EIA month-to-month variations are studied and compared with those derived from the latest version of the IRI-2016 model available at https://ccmc.gsfc.nasa.gov/modelweb/models/iri2016_vitmo.php. The default recommended options are considered for the F-layer peak, bottomside, and topside profiles while running the IRI model. With the currently available larger number of GPS-TEC receivers over Brazil, it is possible

to study the EIA space-time phenomenon in much more detail, with emphasis on the longitudinal variation, which is being investigated in the present paper along with the comparison between observations and IRI-2016 model outputs.

3. Results

3.1. EIA Day-to-Day Variability in Three Different Longitudinal Sectors Over the Brazilian Region

The year 2016 belongs to the descending phase of the Solar Cycle 24 with average F10.7 = 80 s.f.u (1 s.f.u. = 10–22 W m^{-2} Hz^{-1}). This analysis has been carried out with focusing on two different cases of EIA; the first one is when the EIA is developed with clear presence of anomaly crest at low latitudes and trough near geomagnetic equatorial region. The other case is when the EIA is not developed or absent, showing a maximum plasma over the equator and decreasing toward low latitudes. Therefore, to illustrate these two different type of cases, the daily VTEC variations with one case having the EIA developed and other case when the EIA is not developed/absent are presented in Figures 2a and 2b, respectively.

The quiet day of 5 March 2016 is taken as an example to illustrate the space-time evolution of the EIA developed in the three Brazilian longitudinal sectors. The left column of Figure 2a shows the VTEC contour plots as a function of UT and dip latitude/geographic latitude for the west, middle, and east sectors at the top, center, and bottom panels, respectively. The right column of Figure 2a presents the VTEC as a function of dip latitude and geographic latitude at 16:00, 17:00, 18:00, 19:00, 20:00, and 21:00 UT for the considered stations in the west, middle, and east Brazilian sectors.

These contour plots are obtained using VTEC data from a latitudinal chain of GPS-TEC stations distributed from the equatorial region to beyond the anomaly crest in the three sectors considered in this investigation (Figure 1 and Table 1). It is important to mention that VTEC contour plots have a 1-min time resolution.

It is noticed from the reddish patterns that the development of EIA starts around 15:00 UT and reaches its maximum between 17:00 and 18:00 UT, after which it begins to weaken until it disappears around 21:00–22:00 UT. The VTEC variations also indicate that the EIA intensifies from 23:00 to 24:00 UT between −15° and −17° dip latitudes (EIA crest) in the west and middle sectors (indicated by black circle). This is the signature of the equatorial F-layer postsunset height rise due to electric field PRE. The intensification of the eastward electric field at the equatorial region leads to an intensification of the equatorial plasma fountain and consequently a resurgence of the EIA crest at low latitude. For this particular day, the postsunset EIA crest intensification at low latitude takes place only in two sectors, but in some other days, all three sectors have EIA intensification. Since the PRE and postsunset EIA crest intensification relationship is not the subject of this paper, we only call attention for this specific feature just to remind that we are aware of this electrodynamic feature of the equatorial/low-latitude region.

It is possible to see in Figure 2a (top panel) the time evolution and the location of the beginning of the northern EIA ionization crest, trough, and southern ionization crest in the west and middle sectors. In addition, it can be noticed that on 5 March 2016, the crest to trough ratio progressively decreases from west to the east longitudes. This probably indicate that the equatorial plasma fountain effect is stronger in the west sector than in the east sector on this specific day.

In addition, the EIA trough center should be located in geomagnetic equators in the west sector (Figure 2a, upper panels), but it is placed around −2° dip latitude/−11° geographic in the Southern Hemisphere. Since the geomagnetic equator is located between −8° and −9° southward of the geographic equator in the Brazilian west sector (see Figure 1 for more details), the trough of the EIA, seen through VTEC measurements, is located neither in the geographic nor in the geomagnetic equator. This indicates that the EIA location (trough and crests) in the western Brazilian sector is a combination of the photoionization process and equatorial plasma fountain. The western crest of the EIA is located around −14° dip latitude/−21° geographic latitude.

Figure 2a (central panels) for the middle sector presented similar behavior as described in the west sector. It is difficult to specify the position of the EIA trough because the GPS-TEC stations are not well distributed in the equatorial region.

However, in the east sector where both equators are much closer (see Figure 2a, bottom panels), the trough is located around the magnetic equator. Also, the southern EIA crest is located between −8 and −10 dip latitude.

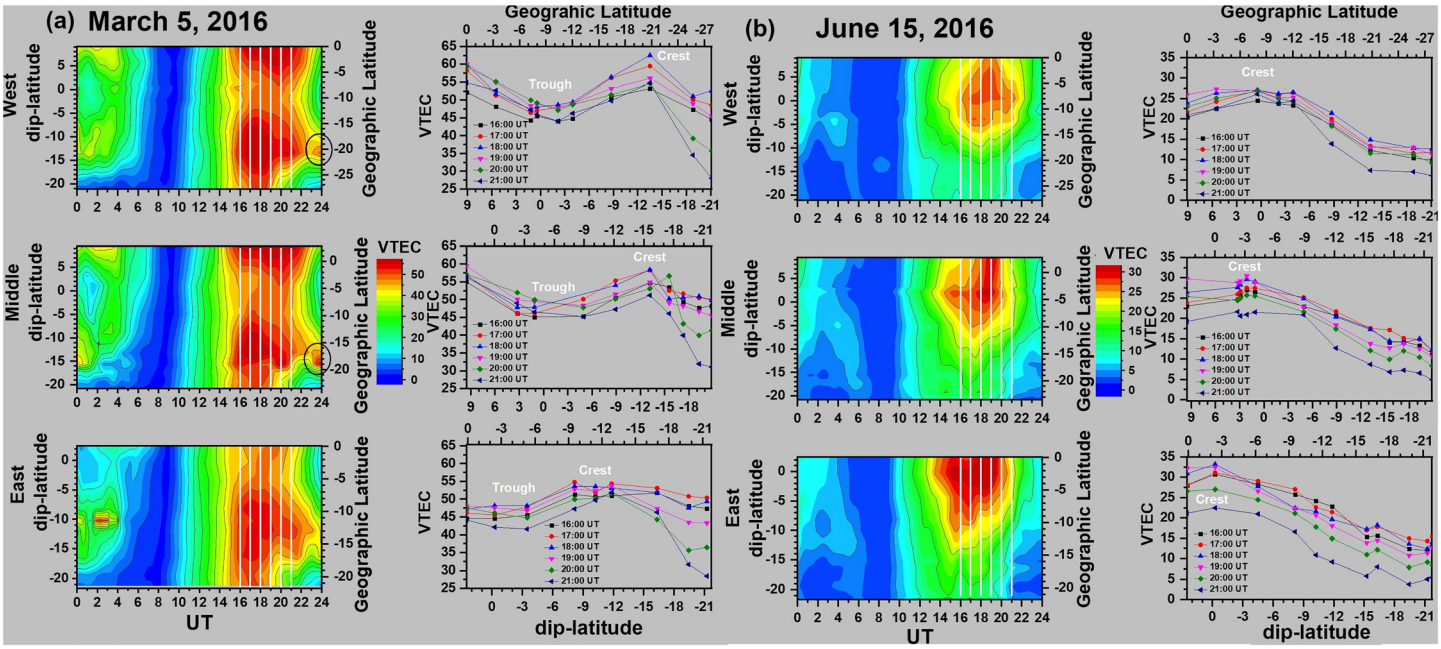

Figure 2. (a) The left panels show the VTEC contour plots of the EIA time evolution in the western, middle, and eastern Brazilian sectors as a function of UT and dip latitude (left *y* axis)/geographic latitude (right *y* axis) on 5 March 2016, when the EIA is developed. The six vertical white lines indicate the time used to show the VTEC as a function of the dip latitude. The right panels show the VTEC variations (raw data) at 16:00, 17:00, 18:00, 19:00, 20:00, and 21:00 UT as a function of the dip latitude (bottom *x* axis)/geographic latitude (top *x* axis). (b) The same as Figure 2a but when the EIA is not developed/absent.

Figure 2b (15 June 2016) shows an example of a day when the EIA is not developed/absent. It is observed that the space–time evolution of the ionization around equator and low latitude is completely different from the previous example when the EIA was developed. Possibly, the fountain effect in this specific day is weaker and does not have sufficient strength to remove the plasma from equatorial region and deposit it at low latitude to form the anomaly crests. Therefore, the ionization produced around the equatorial region is not transported to low latitude, and crest at low latitude is not formed. Consequently, the ionization maximizes over the equator, and it starts to diminish as it moves from the equator to low latitude. However, although the fountain effect has weaker strength and does not uplift the F-layer as much as necessary to form the EIA crests, it was able to spread the ionization for a few degrees on either sides of the dip equator as noted in Figure 2b. For more details about the EIA suppression during disturbed and quiet periods, see Abdu et al. (1991), Fagundes et al. (2016), TakahashiI et al. (1987), and Venkatesh, Fagundes, de Jesus, et al. (2014).

Figure 3 shows the day-to-day occurrence of EIA during the year of 2016, where the red bars, green bars, and white bars indicate developed EIA, not developed/absent, and geomagnetically disturbed days, respectively. Since this investigation is mainly focused on the study of the EIA during quiet days, the geomagnetic disturbed days (Dst < -40 nT) were not taken into account in our analysis.

A perusal in Figure 3 is that from January to April and from September to December, there is more occurrence of developed EIA in the three sectors. On the contrary, from May to August, the number of EIA not developed/absent increased as compared with January–April and September–December.

Table 2 shows the monthly number of cases and percentages within brackets during geomagnetic quiet conditions when the EIA is developed (denoted by Yes) and not developed/absent (denoted by No) for all three sectors studied in this investigation. EIA percentage of occurrence higher than 75% and the EIA not developed/absent higher than 25% are highlighted in red and yellow background, respectively. The monthly percentage of occurrence was calculated using Equation 6.

$$\text{Monthly\%} = \left(\frac{\text{No. of cases}}{\text{Month No. of days} - \text{No. of disturbed days}}\right) \text{x } 100 \tag{6}$$

A semiannual variation is observed on monthly EIA percentage of occurrence with a major maximum

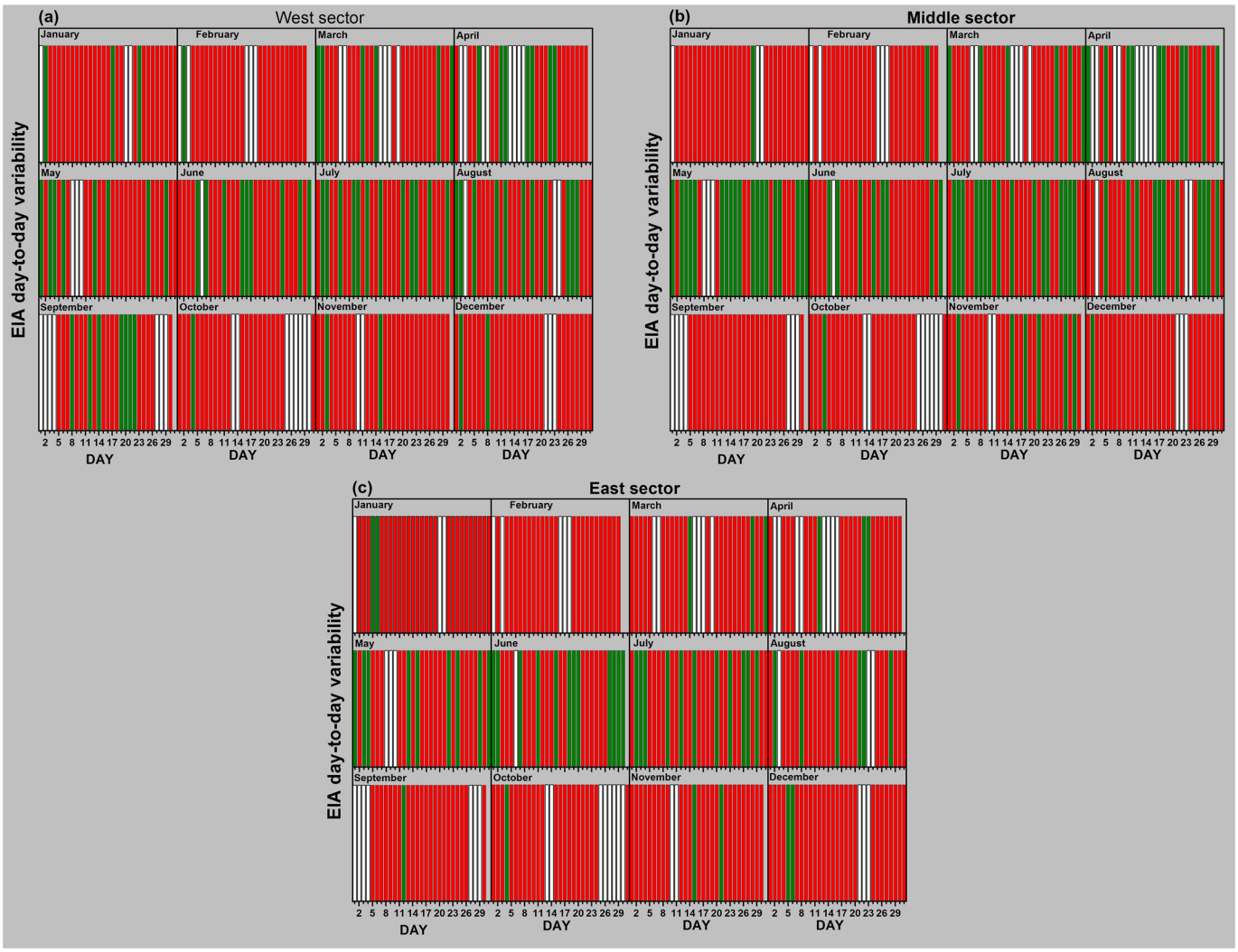

Figure 3. (a) Day-to-day occurrence of the EIA developed (red) and not developed/absent (green) for the west sector during 2016. White bars indicate the disturbed days (Dst < −40 nT). (b) The same as panel (a) but for the middle sector. (c) The same as panel (a) but for the east sector.

around summer and spring and minimum around southern winter However, it is interesting to notice in Table 2 that the number of months that the EIA formed with more than 75% is 6, 7, and 9 in the west, middle, and east sectors, respectively (denoted by red). Besides, the number of months that the EIA is not-developed/absent is 6, 5, and 3 in the west, middle, and east sectors, respectively (denoted by yellow), indicating that there is a longitudinal difference in the EIA formation in the Brazilian sector in the presence of atypical magnetic field structure (large declination of the magnetic equator). This suggests that the photoionization process and the distance between the geographic and geomagnetic equators combined with the fountain effect play an important role in the development of the EIA. The present results of the EIA developed and not-developed occurrence over the Brazilian sector suggest that the longitudinal differences within short separation from the west to the east are related to the geometrical configuration of the magnetic and geographic equators. This is because within this small longitudinal separation, the only parameter that changes significantly is the separation between both equators. Nevertheless, it will be important for model developers to test this hypothesis.

The total number of cases of EIA developed during the year 2016 is 265 (83.6%), 236 (74.4%), and 248 (78.2%), in the east, middle, and west sectors, respectively. When comparing the east-middle and east-west sectors, as expected, the number of days with EIA formed in the east sector is greater than those in the middle and west

Table 2
The Monthly Number of Cases and the Percentage During a Geomagnetic Quiet Period When the EIA is Developed and Not Developed/Absent for the West, Middle, and East Sectors Indicated by Yes and No, Respectively

Month	No. of days	Disturbed days Dst ≤ −40	West		Middle		East	
			Yes (%)	No (%)	Yes (%)	No (%)	Yes (%)	No (%)
Jan	31	3	25 (89.3)	3 (10.7)	27 (96.4)	1 (3.6)	26 (92.9)	2 (7.1)
Feb	29	5	23 (95.8)	1 (4.2)	23 (95.8)	1 (4.2)	24 (100.0)	0 (0.0)
Mar	31	6	19 (76.0)	6 (24.0)	19 (76.0)	6 (24.0)	22 (88.0)	3 (12.0)
Apr	30	8	15 (68.2)	7 (31.8)	11 (50.0)	11 (50.0)	19 (86.4)	3 (13.6)
May	31	3	20 (71.4)	8 (28.6)	9 (32.1)	19 (67.9)	19 (67.9)	9 (32.1)
Jun	30	1	20 (69.0)	9 (31.0)	21 (72.4)	8 (27.6)	17 (58.6)	12 (41.4)
Jul	31	0	19 (61.3)	12 (38.7)	15 (48.4)	16 (51.6)	20 (64.5)	11 (35.5)
Aug	31	3	17 (60.7)	11 (39.3)	17 (60.7)	11 (39.3)	22 (78.6)	6 (21.4)
Sep	30	7	16 (69.6)	7 (30.4)	23 (100.0)	0 (0.0)	22 (95.7)	1 (4.3)
Oct	31	8	22 (95.7)	1 (4.3)	22 (95.7)	1 (4.3)	22 (95.7)	1 (4.3)
Nov	30	2	26 (92.9)	2 (7.1)	22 (78.6)	6 (21.4)	26 (92.9)	2 (7.1)
Dec	31	3	26 (92.9)	2 (7.1)	27 (96.4)	1 (3.6)	26 (92.9)	2 (7.1)
Total	**366**	**49**	**248 (78.2)**	**69 (21.8)**	**236 (74.4)**	**81 (25.6)**	**265 (83.6)**	**52 (16.4)**

Note. The number of days of each month and the number of disturbed days are also shown. The red pattern highlights the months when the EIA development rate is more than 75%, and yellow pattern is when the EIA not developed/absent is more than 25%.

sectors. However, when comparing the central-western sectors, the western sector presents a larger number of days with EIA formed than the central one. It is expected that the western sector has a lesser number of days with EIA formed than the middle sector. Probably, this contradiction of the total number of cases with EIA developed between middle and west sectors must be related to the combination process of photoionization and distance between the geographic and geomagnetic equators that is not well studied actually. Maybe this combination is not a linear function. Therefore, when the number of GPS receivers in the Brazilian equatorial region increases, it will be possible to study the EIA in the Brazilian sector using four or five latitudinal chains of GPS-TEC and explore this contradiction between the middle and west sectors. Consequently, we explore in more detail how the combination of the photoionization process and the distance between the geographic and geomagnetic equators play in the EIA formation and its day-to-day variability.

3.2. Month-to-Month Variations of the EIA Over the Brazilian Sector Using Three GPS-VTEC Networks

In order to study the month-to-month variations of EIA over eastern, middle, and western Brazilian sectors, the monthly mean diurnal variation of VTEC at all stations along the three chains (see Table 1) are computed for the year 2016 (descending phase of the Solar Cycle 24). The monthly mean contour plots of VTEC as a function of UT and dip latitude from January to December are presented in Figures 4a (east), Figure 4b (middle), and Figure 4c (west). The color scale showing the VTEC values ranges from 0 to 50 uniformly for all months and the three sectors.

Around 10:00–11:00 UT, it is possible to notice a transition from dawn (dark blue ~5 TECu) to morning (light blue ~10 TECu and light green ~20 TECu). This color transition is a sign that the photoionization process just started at ionosphere F-layer heights. The electrodynamics related to the fountain effect start at around 12:00 UT and the EIA generation starts at around 13:00–14:00 UT. Finally, a few hours later, the EIA is fully formed (for more details, see Figures 2 and 4). According to Fejer et al. (1979), the vertical drift became positive and the F-layer started its upward lift at around 12:00–13:00 UT (7:00–8:00 LT) in Jicamarca (American sector). Therefore, the present results are supported by the F-layer vertical drift observation made at Jicamarca (Peruvian sector).

A perusal of Figures 4a–4c shows that all sectors have very clear EIA semiannual variations with major maximum VTEC at the crest during January–February–March, minimum during June, July, and August, and

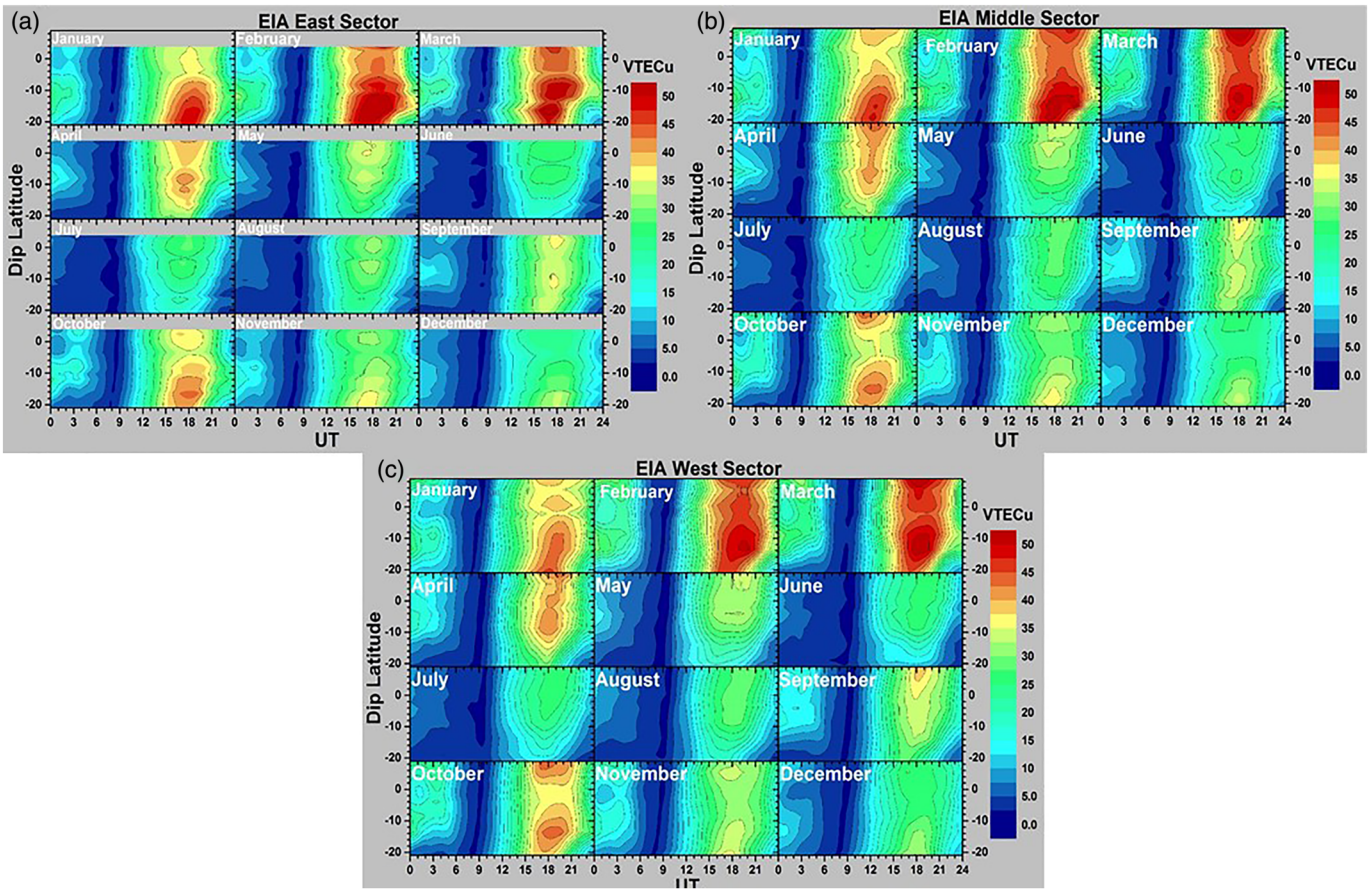

Figure 4. Contour plots showing the averaged VTEC month-to-month variation as a function of UT and dip latitude from January to December 2016. (a) Contour plots showing the EIA month-to-month variability from equator to beyond the EIA crest in the eastern Brazilian sector. (b) The same as Figure 4a but for the middle Brazilian sector. (c) The same as Figure 4a but for the western Brazilian sector.

secondary maximum during September–October–November. In addition, April, May, and December are transition months. The maximum averaged VTEC values are found to be nearly 55 VTECu for a major maximum, 30 VTECu for minimum, and from 40 VTECu for a secondary maximum. It is important to notice that within a short separation between eastern, middle, and western sectors, important differences are seen from month-to-month in the EIA shape and lifetime during the EIA major maximum, minimum, and secondary maximum periods. In addition, the EIA crest and trough month-to-month comparison among the three sectors indicates that the east and west sectors present shape and density intensity (VTEC) are sometimes quite different. However, the middle sector in some months is similar to the east and others are similar to the west sectors.

The seasonal variation of the EIA crest was investigated by several researchers in the Indian, Asian, African, and Brazilian sectors, and semiannual variations have been reported in all these sectors (Amaechi et al., 2019; Bertoni et al., 2006; Huang et al., 2013; Jonah et al., 2015; Kumar et al., 2014; Mo et al., 2018; Rao et al., 2018; Venkatesh, Fagundes, de Jesus, et al., 2014; Zhao et al., 2009). The semiannual peaks in the Chinese and Indian sectors, the Northern Hemisphere, occur during equinox (spring and fall), but in the Brazilian sector, the Southern Hemisphere, the peaks occur during summer and spring/equinox.

Our study indicates that the EIA month-to-month variations in the Brazilian sector differ from the other sectors within a short longitudinal separation, because of the combined effect of the geometry of the geographic and geomagnetic equators and the solar zenith angle (photoionization). To further investigate the EIA differences and similarities in detail, the characteristics of the EIA along the three different longitudinal zones are presented and discussed in the following section.

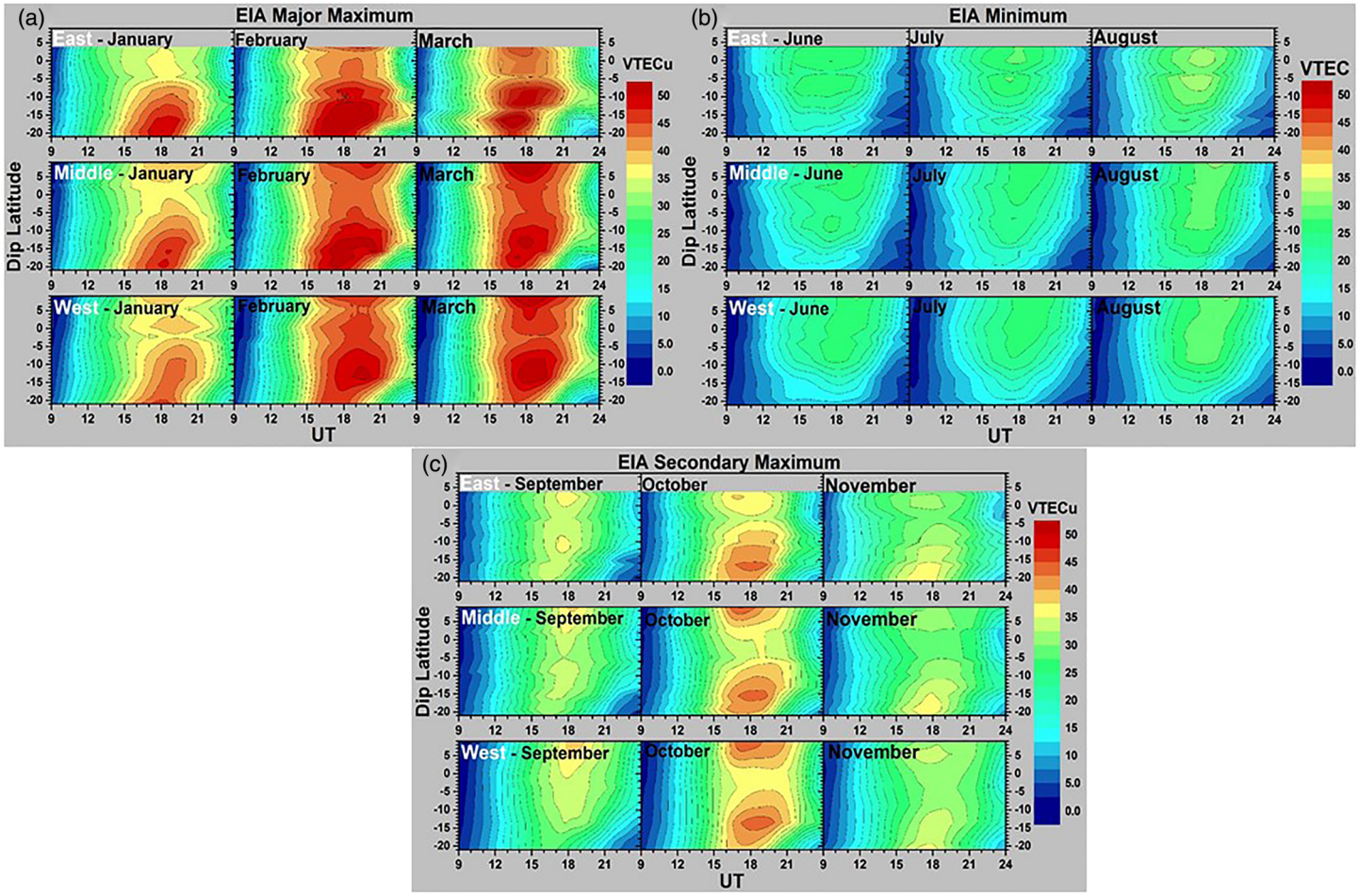

Figure 5. Contour plots showing the monthly mean diurnal variations VTEC as function of UT and dip latitude. (a) For the EIA major maximum (January, February, and March) for eastern (first row), middle (second row), and western (third row) Brazilian sectors. (b) The same as panel (a) but for the EIA minimum (June, July, and August). (c) The same as panel (a) but for the EIA secondary maximum (September, October, and November).

3.3. EIA Comparison Between Eastern, Middle, and Western Brazilian Sectors

To understand the similarities and differences in the EIA features between three sectors, the EIA variations are analyzed during the major maximum (January, February, and March), minimum (June, July, and August), and secondary maximum (September, October, and November) with particular interest on the position and extension of the crest and trough in the Brazilian sector. Figure 5 shows the contour plots of the monthly averages of the VTEC variation as a function of UT and dip latitude at the three sectors during major maximum (Figure 5a), minimum (Figure 5b), and secondary maximum (Figure 5c). The first row of each panel refer to east, the second row to middle, and the third row to west Brazilian sectors. Since the ionization production starts around 06:00 local time only after which the EIA process initiates, these VTEC contour plots are presented from 9:00 UT to 24:00 UT for major maximum, minimum, and secondary maximum.

Figure 5a presents the VTEC variations from 9:00 UT to 24:00 UT showing the EIA during the major maximum (January, February, and March) for the three longitudinal sectors where the VTEC values range from 0 to 50 VTECu. It is seen from this figure that a clear EIA is developed during the 3 months along with the three longitudinal sectors. The EIA crests during January are weaker and have a shorter life than those in February and March in the three sectors.

The EIA crest is found to be comparably weaker in the west sector than that in the middle and east sectors, particularly during January. These variations between the three longitudinal sectors are mainly attributed to

the varied effects of different photochemical and dynamical processes. Probably, the distances between the geographic and geomagnetic is larger in west than that in east sector. The EIA crests in February are stronger and well formed in all sectors.

However, it is interesting notice that the crest-trough-crest separation in the west sector is closer than the middle sector. In March, the EIA structure on the east sector is very complex, showing double south crest, but in the middle and west, the crest presents its standard shape and lifetime. Again, the west trough is narrow as compared with middle sector, and the trough in March is wider and moves to southward as compared with that of February.

Figure 5b shows the EIA during the minimum (June, July, and August) for the three longitudinal sectors, where the VTEC values range from 0 to 50 VTECu. During these 3 months in all sectors, the EIA crests are weaker or not developed and most of the plasma is confined over the geomagnetic equator. In the east sector, the EIA crests are weakly developed in June, July, and August (minimum). Nevertheless, the EIA crest is not developed in the middle and west sectors during the minimum, except on middle June when it is very weakly developed. But it is noticed that the maximum equatorial ionization extends from equatorial region up to low latitudes (~ −10 dip latitude) like a tongue. During the winter time (June, July, and August), the fountain effect is weaker as compared with other seasons and do not have enough strength to form the EIA crest every day as shown in Figure 3. This explains why the EIA crest is weaker or absent during the wintertime.

Figure 5c presents the EIA during the secondary maximum (September, October, and November) for all three sectors where the VTEC value ranges from 0 to 50 TECu. In September, the EIA is weaker developed in the east and middle sectors where the two crests and troughs can be seen, but the lifetime and longitudinal extinction are shorter than those noted during major maximum. However, in the west sector, the EIA is not developed, as the EIA crests and troughs are not seen. It can be seen from Figure 5c that the strongest EIA crests are seen in October during the secondary maximum and they are quite similar for all sectors, but the trough in the middle and west sectors are a little wider than in the east sector. In November, the EIA crest is weaker in all sectors and the trough is wider in all sectors as compared with other October. Similar to the major maximum, the secondary maximum shows a weak signature of the PRE just after the postsunset. Even though the signature is weaker than the major maximum, it is possible to see the EIA secondary intensification just following the isolines in Figure 5c, between 21:00 and 24:00 UT.

In addition, the observed equatorial trough during the major maximum is longer than those observed during the secondary maximum (Figure 5c). Which means that the crests are quite well separated during the major maximum. This is probably being caused by the combination of strong fountain effect with solar zenith angle during summer and the large distance between the geographic and geomagnetic equators. It is observed in Figure 5a that during the EIA major maximum, there is a clear difference between the formation (around 15:00 UT) and decay (around 22:00 UT) in EIA crest development. The development of the EIA crest increases rapidly, but the decay of EIA takes place more gradually. This feature is seen in all three sectors with different strengths and time durations. The gradual decrease in the EIA crest during the final stages is the signature of the PRE that takes place during the sunset hours.

The detailed comparison of EIA features between three sectors during different months indicates significant month-to-month and seasonal variations on the strength as well as the extent of EIA crests and troughs. It is known that the EIA variability is effected by several factors such as the fountain effect, neutral winds, and photochemical processes (Luan et al., 2015; Tulasi Ram et al., 2009). One of the striking factors between these closely separated longitudinal sectors is the distance between geographic and geomagnetic equators due to the uniquely inclined structure of the geomagnetic field lines. In the west sector, the separation between two equators is large, while they are comparably closer in the east sector. Therefore, the fountain effect in the west sector originates from a farther distance of geographic equator where the production is maximum. In addition, the effects of different factors on EIA behaviors are changed with the displacement of the geographic and geomagnetic equators combined with neutral winds (Su et al., 1997). Thus, the varied effects of photochemical and fountain processes due to large differences between geographic and geomagnetic equators during different seasons must have resulted in significant variabilities in the characteristics of EIA between the three sectors.

3.4. Comparison Between the GPS and IRI Model Derived EIA Features

The IRI model 2016 (https://ccmc.gsfc.nasa.gov/modelweb/models/iri2016_vitmo.php; Bilitza, 2001, 2018) is most widely used model to derive the VTEC values. With a view to understand whether the IRI modeled EIA shows above observed significant differences between the three sectors, the TEC values for all the stations used in this work (Figure 1 and Table 1) are estimated using the online version of IRI. The IRI-2016 model default options such as "URSI" for "Ne F-peak"; "NeQuick" for "Ne Topside"; "AMBT-2013" for "F-peak height"; and "ABT-2009" for "Bottom side thickness" are considered while running the model. A comparative analysis has been made between the EIA features using the observed GPS-VTEC data and the IRI-2016 modeled TEC for the three Brazilian sectors.

It can be noticed from Figure 1a that the GPS receiver locations in any of the chain are not exactly equally separated and not perfectly aligned on the straight line perpendicular to magnetic equator. In order to make sure that the EIA features from the monthly mean diurnal contours of the IRI modeled TEC in the eastern, middle, and western Brazilian sectors are appropriate to compare with the contour plots of GPS TEC variations, the following test was made using IRI-2016 model derived VTEC values.

First, the monthly mean diurnal variations of IRI-TEC values for February are calculated for the same coordinates of those stations that were used for the west GPS-TEC network (yellow icons in Figure 6a). In addition, the monthly mean diurnal variations of IRI-TEC during February are calculated for an ideal case in such a way that the considered locations along the chain are equally spaced and exactly on the white line perpendicular to the geomagnetic equator (blue icons in Figure 6a).

Figure 6b (upper panels) shows the EIA (crest and trough) for a set of coordinates equally spaced on the white line, and Figure 6b (bottom panels) shows the results for a set of stations that have the same coordinates of the GPS-TEC stations. It is clearly noticed that both VTEC contour plots derived from IRI-TEC model are quite similar. It is important to mention that the monthly mean IRI-TEC diurnal values are calculated using Days 5, 10, 15, and 25 for each station with the time resolution of 25 min. Those monthly mean IRI-TEC values at different stations are used to generate EIA contours as a function of UT and dip latitude for the three sectors.

The EIA morphologies (crest and trough) seen through the measured GPS-TEC and IRI-TEC model values are quite different. When we compare the contour plots (Figures 4 and 7), it is possible to notice that the EIA seen through GPS-TEC model data are more elongated in latitude than it is seen in IRI-TEC, which presents an oval shape. In addition, the EIA (IRI-TEC) presents a crest and a trough which are more defined.

Figure 7 shows the EIA contour plots of IRI-2016 modeled monthly mean TEC as a function of UT and dip latitude for the eastern, middle, and western Brazilian sectors for the same station coordinates that were used in the three GPS-TEC networks (Table 1).

It is noticed that the monthly mean diurnal variations contour plots derived from IRI-TEC model for east, middle, and west sectors are quite similar. Therefore, the IRI model did not capture properly the EIA east-west differences in the Brazilian sector. Probably, IRI-TEC model needs some improvement to take into account the specificities of the geometric configuration between the geographic and magnetic equators in the Brazilian sector. Therefore, comparisons between the EIA monthly mean diurnal variations obtained from experimental measured GPS-VTEC and derived IRI-TEC model data using the available stations close to the black lines on in Figure 1 are useful to estimate the performance of IRI-2016 model to predict the EIA (crest and trough) in the Brazilian sector (Figure 7).

The contour plots of IRI modeled VTEC along the three sectors have shown semiannual behavior in the strength of the EIA as seen in GPS-TEC variations. However, the months of the occurrence of major maximum, minimum, and secondary maximum are different between observation and model outputs. In the IRI modeled outputs, the major maximum of EIA strength is seen during the equinoctial months of March, April, September, and October with the secondary maximum during November, December, January, and February. These months of the occurrence of EIA main and secondary maximum are not exactly coinciding with the GPS observations. However, the EIA minimum in IRI modeled TEC is seen during June, July, and August, which is in agreement with the observations.

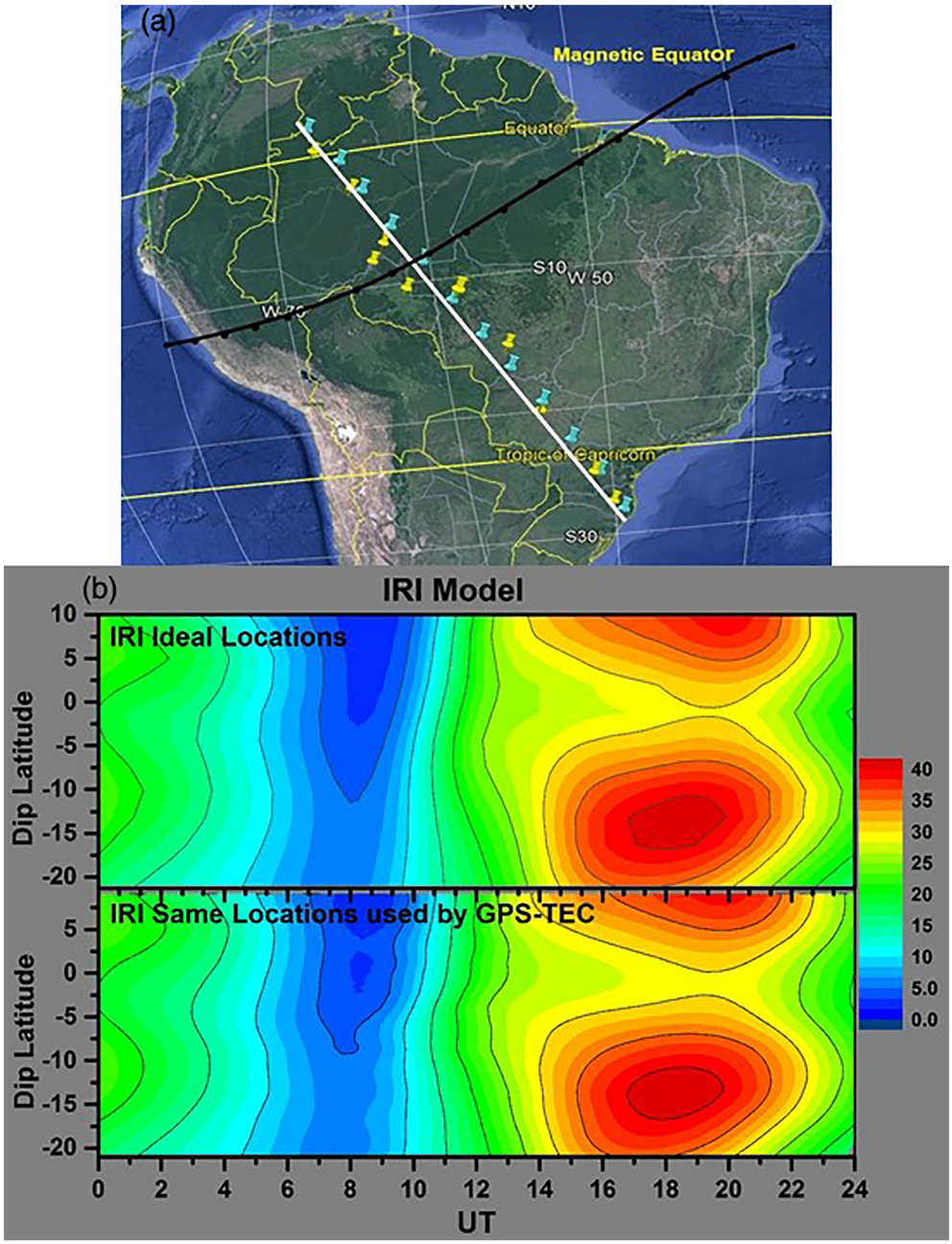

Figure 6. (a) Map showing the 12 locations used for an ideal case where all considered locations are equally spaced and exactly on the white line (blue icons). Yellow icons show the 10 locations of the GPS TEC receivers used for the west sector. (b) Contour plots showing the monthly mean IRI-TEC variations for February as function of UT and dip latitude. The upper panel shows the EIA derived from IRI-TEC values for ideal locations and the bottom panel shows the EIA features derived from IRI model using the GPS-TEC network locations.

The EIA morphologies (crest and trough) seen through the measured GPS-TEC and IRI-TEC model values are quite different. When we compare the contour plots (Figures 3 and 6), it is possible to notice that the EIA seen through GPS-TEC model data are more elongated in latitude than it is seen in IRI-TEC, which presents an oval shape. In addition, the EIA (IRI-TEC) presents a crest and a trough which are more defined. On the other hand, the EIA trough (GPS-TEC) is not always localized at the magnetic equator and is larger than that predicted by the IRI-TEC model results.

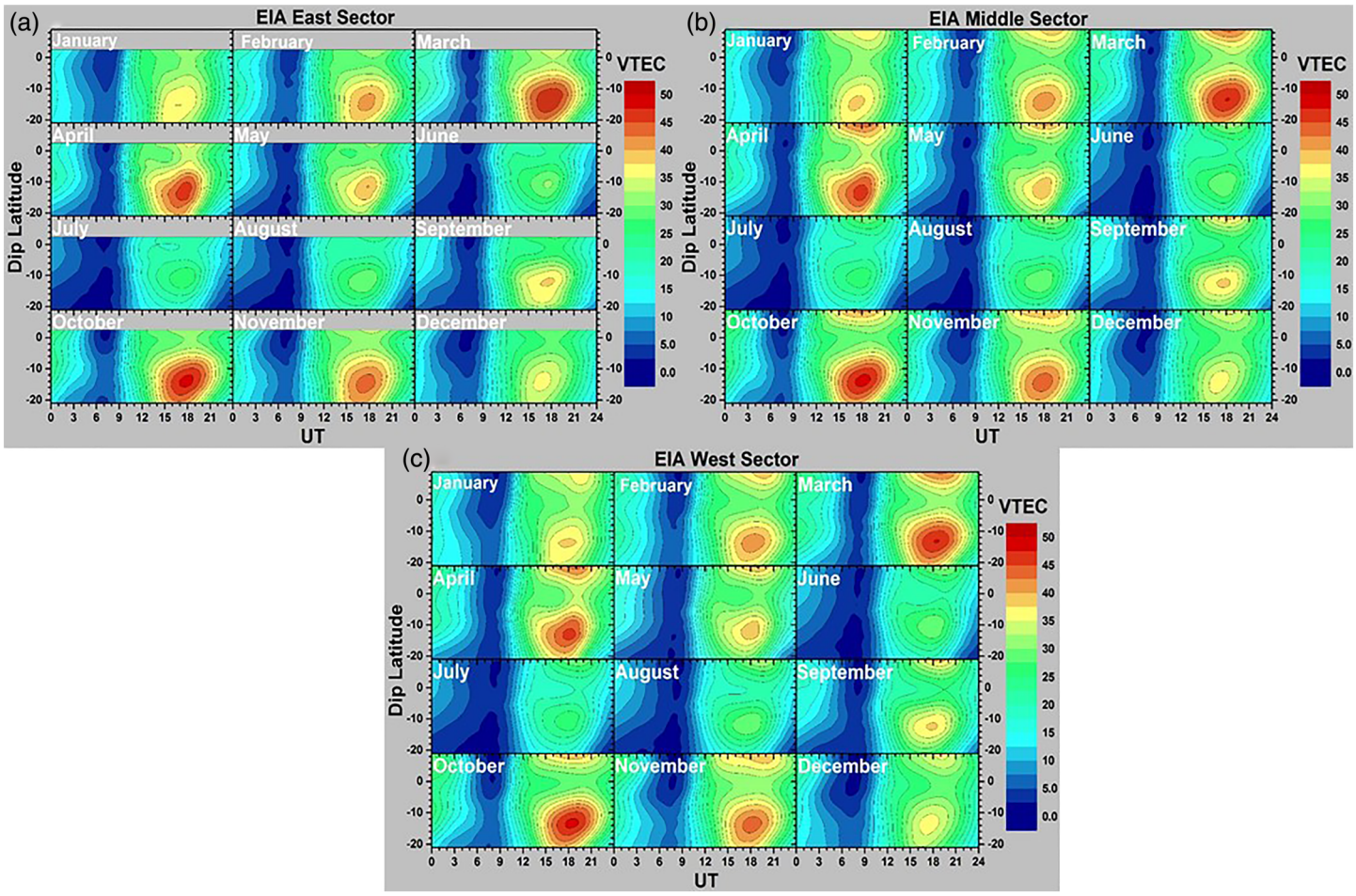

Figure 7. Contour plots showing the averaged IRI-VTEC month-to-month variation as a function of UT and dip latitude from January to December 2016. (a) Contour plots showing the EIA month-to-month variability from equator to beyond the EIA crest in the eastern Brazilian sector. (b) The same as Figure 7a but for the middle Brazilian sector. (c) The same as Figure 7a but for the western Brazilian sector.

A comparison between GPS-VTEC with model-derived IRI-2012 TEC values in Palmas (10.2°S, dip latitude 5.5°S, near equatorial region) and Sao Jose Campos (23.2°S, dip latitude 17.6°S, under the EIA crest) stations for low solar activity (LSA) in the Brazilian sector is made by De Abreu et al. (2017). They noticed that IRI-TEC model and GPS-TEC showed better agreement during the nighttime. However, during daytime and evening, the IRI-TEC and GPS-VTEC or foF2 showed larger differences (De Abreu et al., 2017; Perna et al., 2018; Venkatesh, Fagundes, de Jesus, et al., 2014; Venkatesh, Fagundes, Seemala, et al., 2014). Rao et al. (2018) investigated the foF2 in the Chinese low-latitude sector and noticed significant discrepancy in the foF2 values from ionosonde and IRI 2016 model. They noticed that the IRI 2016 model underestimates the foF2 values in winter and equinoxes and overestimates foF2 values in summer.

Further, it is noticed that the monthly mean diurnal variations contour plots from IRI model for east, middle, and west sectors are quite similar in contrast to the significant differences in the observations. This shows that the IRI model did not capture properly the EIA east-west differences in the Brazilian sector. Probably, IRI-TEC model needs some improvement to take into account the specifications of the geometric configuration between the geographic and magnetic equators in the Brazilian sector. Therefore, comparisons between the EIA monthly mean diurnal variations obtained from experimental measured GPS-VTEC and derived IRI-TEC model data using the available stations close to the black lines on in Figure 1 are useful to estimate the performance of IRI-2016 model to predict the EIA (crest and trough) in the Brazilian sector.

4. Conclusions

The EIA crest is found to be comparably weaker in the west sector than that in the middle and east sectors, particularly during January. These variations between the three longitudinal sectors are mainly attributed to the varied effects of different photochemical and dynamical processes, probably due to the distances between the geographic and geomagnetic equators which are larger in west than that in east sector. The EIA crests in February are stronger and well formed in all sectors.

1. Daily and monthly EIA variations over the Brazilian east, middle, and west sectors show a semiannual variation. All sectors show a major maximum during the summer (January, February, and March), a minimum during the winter (June, July, and August), and secondary maximum during spring (September, October, and November).
2. We investigated the day-to-day occurrence of the EIA developed and not developed/absent for the west, middle, and east sectors during the quiet period. The number of days with EIA developed and not developed/absent during quiet period has shown longitudinal dependence. The number of months having more than 75% of EIA developed days are found to increase from west to east Brazilian sectors.
3. The EIA crests during January are weaker and have a shorter lifetime than those in February and March in the three sectors. The EIA crests in February are stronger and well-formed in all sectors. The EIA crest is found to be comparably weaker in the west sector than that in the middle and east sectors, particularly during January. The EIA during the major maximum show longer equatorial trough than those observed during the secondary maximum.
4. During the EIA minimum months (June, July, and August), the EIA crests are not developed or weaker than in other months. In June, the EIA is not developed at all in the east sector but is weakly developed in middle and west sectors, and the trough in the middle and west sectors are narrow. In August, the EIA crest does not form in any of the three sectors.
5. During the secondary maximum, the strongest EIA crests noticed in October and EIA are quite similar to all sectors, but the troughs in the middle and west sectors are longer than the east sector.
6. The months of occurrence of EIA major maximum and secondary maximum in the IRI-2016 model are not coinciding with the GPS TEC observations while the EIA minimum is seen during similar months from both observations and model. The EIA crest in the GPS observations is attitudinally more elongated, while the IRI model presents it in an oval shape. On the other hand, the EIA trough (GPS-TEC) is not localized to the magnetic equator and is larger than that predicted by the (IRI-TEC) model. Particularly, the significant differences in the EIA features between three sectors observed in the experimentally derived GPS TEC are not seen in the IRI-2016 model outputs.

Acknowledgments

We wish to express our sincere thanks to the State of Sao Paulo Research Foundation (FAPESP) for financial support through the Process No. 2016/10495-5 and No. 2012/08445-9 and Conselho Nacional de Desenvolvimento Científico e Tecnológico (CNPq) Process No. 302406/2017-4. One of the authors (K. V.) acknowledges the National Atmospheric Research Laboratory (NARL), India, for support through fellowship. The authors wish to express their sincere thanks to the IBGE (http://www.ibge.gov.br/home/geociencias/geodesia/rbmc/rbmc_est.php) for providing dual frequency GPS data Brazil and IRI model 2016 (https://ccmc.gsfc.nasa.gov/modelweb/models/iri2016_vitmo.php).

References

Abdu, M. A., Batista, I. S., & de Souza, J. R. (1996). An overview of IRI-observational data comparison in American (Brazilian) sector low latitude ionosphere. *Advances in Space Research*, *18*(6), 13–22. https://doi.org/10.1016/0273-1177(95)00893-4

Abdu, M. A., Sobral, J. H. A., DePaula, E. R., & Batista, I. S. (1991). Magnetospheric disturbance effects on the equatorial ionization anomaly (EIA)—An overview. *Journal of Atmospheric and Solar-Terrestrial Physics*, *53*(8), 757–771. https://doi.org/10.1016/0021-9169(91)90126-R

Adebesin, B. O., Rabiu, A. B., Bolaji, O. S., Adeniyi, J. O., & Amory-Mazaudier, C. (2018). Ionospheric climatology at Africa EIA trough stations during descending phase of sunspot cycle 22. *Journal of Atmospheric and Solar-Terrestrial Physics*, *172*, 83–99. https://doi.org/10.1016/j.jastp.2018.03.009

Amaechi, P. O., Oyeyemi, E. O., & Akala, A. O. (2019). Variability of the African equatorial ionization anomaly (EIA) crests during the year 2013. *Canadian Journal of Physics*, *97*, 155–165. https://doi.org/10.1139/cjp-2017-0985

Appleton, E. V. (1946). Two anomalies in the ionosphere. *Nature*, *157*, 691–693. https://doi.org/10.1038/157691a0

Batista, I. S., & Abdu, M. A. (2004). Ionospheric variability at Brazilian low and equatorial latitudes: Comparison between observations and IRI model. *Advances in Space Research*, *34*(9), 1894–1900. https://doi.org/10.1016/j.asr.2004.04.012

Batista, I. S., de Souza, J. R., Abdu, M. A., & de Paula, E. R. (1994). Total electron content at low latitudes and its comparison with IRI90. *Advances in Space Research*, *14*(12), 87–90. https://doi.org/10.1016/0273-1177(94)90246-1

Bertoni, F., Sahai, Y., Lima, W. L. C., Fagundes, P. R., Pillat, V. G., Becker-Guedes, F., & Abalde, J. R. (2006). IRI-2001 model predictions compared with ionospheric data observed at Brazilian low latitude stations. *Annales de Geophysique*, *24*(8), 2191–2200. https://doi.org/10.5194/angeo-24-2191-2006

Bhuyan, P. K., & Borah, R. R. (2007). TEC derived from GPS network in India and comparison with IRI. *Advances in Space Research*, *39*(5), 830–840. https://doi.org/10.1016/j.asr.2006.12.042

Bilitza, D. (2001). International Reference Ionosphere 2000. *Radio Science*, *36*(2), 261–275. https://doi.org/10.1029/2000RS002432

Bilitza, D. (2018). IRI the international standard for the ionosphere. *Advances in Radio Science*, *16*, 1–11. https://doi.org/10.5194/ars-16-1-2018

Bilitza, D., Hernández-Pajares, M., Juan, J. M., & Sanz, J. (1998). Comparison between IRI and GPS-IGS derived electron content during 1991–97. *Physics and Chemistry of the Earth*, *24*(4), 311–319. https://doi.org/10.1016/S1464-1917(99)00004-5

de Abreu, A. J., Martin, I. M., de Jesus, R., Bolzan, M. J. A., Venkatesh, K., Fagundes, P. R., et al. (2017). Comparison of GPS-TEC measurements with IRI2012-TEC predictions in the Brazilian sector during the unusual solar minimum 2009. *Annales de Geophysique*, *60*, A0331. https://doi.org/10.4401/ag-7300

Fagundes, P. R., Cardoso, F. A., Fejer, B. G., Venkatesh, K., Ribeiro, B. A. G., & Pillat, V. G. (2016). Positive and negative GPS-TEC ionospheric storm effects during the extreme space weather event of March 2015 over the Brazilian sector. *Journal of Geophysical Research: Space Physics*, *121*, 5613–5625. https://doi.org/10.1002/2015JA022214

Fejer, B. G., Farley, D. T., Woodman, R. F., & Calderon, C. (1979). Dependence of equatorial F-region vertical drifts on season and solar-cycle. *Journal of Geophysical Research*, *84*(10), 5792–5796. https://doi.org/10.1029/JA084iA10p05792

Huang, L. F., Huang, J., Wang, J. S., Jiang, Y., Deng, B. C., Zhao, K., & Lin, G. G. (2013). Analysis of the north-south asymmetry of the equatorial ionization anomaly around 110 degrees E longitude. *Journal of Atmospheric and Solar-Terrestrial Physics*, *102*, 354–361. https://doi.org/10.1016/j.jastp.2013.06.010

Jonah, O. F., de Paula, E. R., Muella, M. T. A. H., Dutra, S. L. G., Kherani, E. A., Negreti, P. M. S., & Otsuka, Y. (2015). TEC variation during high and low solar activities over South American sector. *Journal of Atmospheric and Solar-Terrestrial Physics*, *135*, 22–35. http://doi.org/10.1016/j.jastp.2015.10.005

Khadka, S. M., Valladares, C. E., Sheehan, R., & Gerrard, A. J. (2018). Effects of electric field and neutral wind on the asymmetry of equatorial ionization anomaly. *Radio Science*, *53*, 683–697. http://doi.org/10.1029/2017RS006428

Kumar, S., Singh, A. K., & Lee, J. (2014). Equatorial ionospheric anomaly (EIA) and comparison with IRI model during descending phase of solar activity (2005–2009). *Advances in Space Research*, *53*, 724–733. http://doi.org/10.1016/j.asr.2013.12.019

Luan, X., Wang, P., Dou, X. K., & Liu, Y. C.-M. (2015). Interhemispheric asymmetry of the equatorial ionization anomaly in solstices observed by COSMIC during 2007–2012. *Journal of Geophysical Research: Space Physics*, *120*, 3059–3073. https://doi.org/10.1002/2014JA020820

Mo, X. H., Zhang, D. H., Liu, J., Hao, Y. Q., Ye, J. F., Qin, J. S., et al. (2018). Morphological characteristics of equatorial ionization anomaly crest over Nanning region. *Radio Science*, *53*, 37–47. http://doi.org/10.1002/2017RS006386

Oluwadare, T. S., Thai, C. N., Akala, A. O. O., Heise, S., Alizadeh, M., & Schuh, H. (2019). Characterization of GPS-TEC over African equatorial ionization anomaly (EIA) region during 2009–2016. *Advances in Space Research*, *63*, 282–301. http://doi.org/10.1016/j.asr.2018.08.044

Oyekola, O. S., & Fagundes, P. R. (2012). Equatorial F-2-layer variations: Comparison between F-2 peak parameters at Ouagadougou with the IRI-2007 model. *Earth, Planets and Space*, *64*(6), 553–566. https://doi.org/10.5047/eps.2011.07.017

Perna, L., Venkatesh, K., Pillat, V. G., Pezzopane, M., Fagundes, P. R., Ezquer, R. G., & Cabrera, M. A. (2018). Bottom side profiles for two close stations at the southern crest of the EIA: Differences and comparison with IRI-2012 and NeQuick2 for low and high solar activity. *Advances in Space Research*, *61*, 295–315. http://doi.org/10.1016/j.asr.2017.10.007

Prasad, S. N. V. S., Rao, P. V. S. R., Prasad, D. S. V. V. D., Venkatesh, K., & Niranjan, K. (2012). On the variabilities of the total electron content (TEC) over the Indian low latitude sector. *Advances in Space Research*, *49*(5), 898–913. http://doi.org/10.1016/j.asr.2011.12.020

Rama Rao, P. V. S., Gopi Krishna, S., Niranjan, K., & Prasad, D. S. V. V. D. (2006). Temporal and spatial variation in TEC using simultaneous measurements from the Indian GPS network of receivers during the low solar activity period of 2004–2005. *Annales de Geophysique*, *24*, 3279–3292. http://doi.org/10.5194/angeo-24-3279-2006

Rao, S. S., Chakraborty, M., & Pandey, R. (2018). Ionospheric variations over Chinese EIA region using foF2 and comparison with IRI-2016 model. *Advances in Space Research*, *62*, 84–93. http://doi.org/10.1016/j.asr.2018.04.009

Ribeiro, B. A. G., Fagundes, P. R., Venkatesh, K., Tardelli, A., Pillat, V. G., & Seemala, G. K. (2019). Equatorial and low-latitude positive ionospheric phases due to moderate geomagnetic storm during high solar activity in January 2013. *Advances in Space Research*, *64*, 995–1010. https://doi.org/10.1016/j.asr.2019.05.032

Romero-Hernandez, E., Denardini, C. M., Takahashi, H., Gonzalez-Esparza, J. A., Nogueira, P. A. B., de Padua, M. B., et al. (2018). Daytime ionospheric TEC weather study over Latin America. *Journal of Geophysical Research: Space Physics*, *123*, 10,345–10,357. https://doi.org/10.1029/2018JA025943

Seba, E. B., Nigussie, M., & Moldwin, M. B. (2018). The relationship between equatorial ionization anomaly and nighttime equatorial spread F in East Africa. *Advances in Space Research*, *62*, 1737–1752. http://doi.org/10.1016/j.asr.2018.06.029

Seemala, G. K., & Valladares, C. E. (2011). Statistics of total electron content depletions observed over the South American continent for the year 2008. *Radio Science*, *46*, RS5019. https://doi.org/10.1029/2011RS004722

Su, Y. Z., Bailey, G. J., Oyama, K. I., & Balan, N. (1997). A modeling study of the longitudinal variations in the north-south asymmetries of the ionospheric equatorial anomaly. *Journal of Atmospheric and Solar-Terrestrial Physics*, *59*, 1299–1310. https://doi.org/10.1016/S1364-6826(96)00016-8

TakahashiI, T., Oya, H., & Watanabe, S. (1987). Ionospheric disturbances induced by substorm associated electric-fields in the low-latitude F-region. *Journal of Geomagnetism and Geoelectricity*, *39*(4), 187–209. https://doi.org/10.5636/jgg.39.187

Tardelli, A., Pezzopane, M., Fagundes, P. R., Venkatesh, K., Pillat, V. G., Cabrera, M. A., & Ezquer, R. G. (2018). Study of the F3 and StF4 layers at Tucuman near the southern crest of the equatorial ionization anomaly in western South America. *Journal of Geophysical Research: Space Physics*, *123*, 2156–2167. http://doi.org/10.1002/2017JA024539

Tulasi Ram, S., Su, S. Y., & Liu, C. H. (2009). FORMOSAT-3/COSMIC observations of seasonal and longitudinal variations of equatorial ionization anomaly and its interhemispheric asymmetry during the solar minimum period. *Journal of Geophysical Research*, *114*, A06311. https://doi.org/10.1029/2008JA013880

Venkatesh, K., Fagundes, P. R., de Jesus, R., de Abreu, A. J., Pillat, V. G., & Sumod, S. G. (2014). Assessment of IRI-2012 profile parameters by comparison with the ones inferred using NeQuick2, ionosonde and FORMOSAT-1 data during the high solar activity over Brazilian equatorial and low latitude sector. *Journal of Atmospheric and Solar-Terrestrial Physics*, *121*, 10–23. http://doi.org/10.1016/j.jastp.2014.09.014

Venkatesh, K., Fagundes, P. R., Seemala, G. K., de Jesus, R., de Abreu, A. J., & Pillat, V. G. (2014). On the performance of the IRI-2012 and NeQuick2 models during the increasing phase of the unusual 24th solar cycle in the Brazilian equatorial and low-latitude sectors. *Journal of Geophysical Research: Space Physics*, *119*, 5087–5105. https://doi.org/10.1002/2014JA019960

Vieira, F., Fagundes, P. R., Venkatesh, K., Goncharenko, L. P., & Pillat, V. G. (2017). Total electron content disturbances during minor sudden stratospheric warming, over the Brazilian region: A case study during January 2012. *Journal of Geophysical Research: Space Physics*, *122*, 2119–2135. http://doi.org/10.1002/2016JA023650

Zhao, B., Wan, W., Liu, L., & Ren, Z. (2009). Characteristics of the ionospheric total electron content of the equatorial ionization anomaly in the Asian-Australian region during 1996-2004. *Annales de Geophysique*, *27*(10), 3861–3873. http://doi.org/10.5194/angeo-27-3861-2009